Tracing circumnuclear dense gas in H$_2$O maser galaxies

A. Farhan[1]⋆, E. N. Ercan[1]† and F. Tombesi[2,3,4,5]‡

[1]*Department of Physics, Bogazici University, Istanbul, 34342, Turkey*
[2]*Department of Physics, Tor Vergata University of Rome, Via della Ricerca Scientifica 1, 00133 Rome, Italy*
[3]*INAF - Astronomical Observatory of Rome, Via Frascati 33, 00044 Monte Porzio Catone, Rome, Italy*
[4]*Department of Astronomy, University of Maryland, College Park, MD 20742, USA*
[5]*X−ray Astrophysics Laboratory, NASA/Goddard Space Flight Center, Greenbelt, MD 20771, USA*

ABSTRACT

A sample of 30 H$_2$O extra-galactic maser galaxies with their published HCN(J=1−0) and HCO+(J=1−0) observations has been compiled to investigate the dense gas correlation with H$_2$O maser emission. Our sample number exceeds the size of the previous HCN samples studied so far by a factor of three, and it is the first study on the possible relation with the dense gas tracer HCO+. We find a strong correlation between normalized H$_2$O maser emission luminosity (L$_{\rm H_2O}$/L$_{\rm CO}$) and normalized HCO+ line luminosity (L$_{\rm HCO+}$/L$_{\rm CO}$). Moreover, a weak correlation has been found between L$_{\rm H_2O}$/L$_{\rm CO}$ and normalized HCN line luminosity (L$_{\rm HCN}$/L$_{\rm CO}$). The sample is also studied after excluding Luminous and Ultraluminous infrared galaxy (U)LIRG sources, and the mentioned correlations are noticeably stronger. We show that 'Dense gas' fractions as obtained from HCN and HCO+ molecules tightly correlate with maser emission, especially for galaxies with normal IR luminosity(L$_{\rm IR}$< 10^{11}L$_\odot$) and we show that HCO+ is a better 'dense gas' tracer than HCN. Further systematic studies of these dense gas tracers with higher transition level lines are vital to probe megamaser physical conditions and to accurately determining how maser emission interrelates with the dense gas.

Key words: masers – galaxies: active – galaxies: star formation – infrared: galaxies – methods: data analysis.

1 INTRODUCTION

Since the discovery of extragalactic water maser galaxies (emitting at $\nu = 22.2$ GHz, $\lambda = 1.35$ cm) by Churchwell et al. (1977), several surveys have been conducted using different constraints on the chosen samples, e. g. X-ray spectrum, hydrogen column density, and nuclear radio continuum. Such constraints have been considered to increase the detection rate.

Megamaser host galaxies have been found to have complex X-ray spectra together with higher X-ray luminosities than non-maser galaxies (e.g. Kondratko et al. 2006; Leiter et al. 2017). Also the megamaser sources have been found to preferably exist in galaxies with high hydrogen column density (N$_{\rm H}$ ≥10^{22} cm^{-2}) due to the connection of masing spots with a highly obscured region near the accretion disk as discussed by Braatz et al. (1997), Zhang et al. (2006), Greenhill et al. (2008), and Castangia et al. (2013). Most commonly, maser emission is observed in Seyfert 2 or Low Ionization Nuclear Emission-Line Region (LINER) type of galaxies (see e.g. Braatz et al. 1997; Lo 2005). Recent studies show that megamaser galaxies have 2-3 orders of magnitude higher nuclear radio continuum luminosities than non-masers (see e.g. Zhang et al. 2012; Liu et al. 2016).

However, the detection rate found so far is still low: of the order of 3 per cent. In fact, from roughly 6000 galaxies surveyed for H$_2$O megamasers (H$_2$OMM) there are only 180 detected as recently reported by Kuo et al. (2020).

The low detection rate of H$_2$OMM was the motivation for several researchers to suggest other possible search criteria (Zhang et al. 2006; Greenhill et al. 2008; Zhang et al. 2009; Ramolla et al. 2011; Zhu et al. 2011; Constantin A. 2012; Van den Bosch et al. 2016; Liu et al. 2017; Kuo C. Y., et al. 2018).

It was proposed by Claussen & Lo (1986) that luminous H$_2$OMM form in dense gas clouds (n(H$_2$)≥10^4 cm^{-3}) in the circumnuclear disks (CND) of Active Galactic Nuclei (AGN), fuelled by accretion. Therefore, dense gas tracers were suggested to be a suitable indicator of H$_2$O masers (Zhang et al. 2009) since they track high density and tem-

⋆ E-mail: ahlamfarhan@yahoo.com (AF)
† ercan@boun.edu.tr (ENE)
‡ francesco.tombesi@roma2.infn.it (FT)

perature molecular clouds excited by collisions. Amongst the most abundant dense gas tracers in galaxies is HCN with a large dipole moment ($\mu \approx 2.98$ Debye D) and it can be thermalised by collisions at high densities, with a critical density of $n_{crit} \sim 10^6$ cm^{-3} at which the spontaneous emission rate equals to the collisional transition rate (see e.g. Baan et al. 2008). HCO+ is another dense gas tracer with a dipole moment $\mu \sim 3.92$ D, and $n_{crit} \sim 10^5$ cm^{-3}.

Thanks to the large HCN survey published by Gao & Solomon (2004), Huang et al. (2014) were able to study the possible correlation between dense gas tracers and maser emission, finding a positive correlation. However, their sample was limited to 13 galaxies. In this work, we increased the sample to 30 galaxies with HCN observations, moreover, this is the first work studying the possible correlations between maser emission and another dense gas tracer, specifically HCO+.

In Section 2 we describe the sample and its corresponding data. Analyses and results of non-parametric statistical approaches to the sample are presented in Section 3. Discussion of the results is presented in Section 4 while main results are summarized in Section 5. Throughout our analyses we adopt flat cosmology parameters of ($\Omega_m = 0.27$, $\Omega_\Lambda = 0.73$, and $H_0 = 71$ kms^{-1}Mpc^{-1}); Spergel et al. (2007). Wherever CO, HCN, or HCO+ appear in this work, we mean the first rotational excitation J-transition emission lines, in other words, CO(J=1-0), HCN(J=1-0) and HCO+(J=1-0), respectively, unless other line is explicitly mentioned.

2   DATASET

There are about 180 known H_2O galaxies so far. A catalog of 22 GHz H_2OMM galaxies was updated by Jim Braatz at the National Radio Astronomy Observatory (NRAO)[1]. We checked the line emissions of HCN(J=1-0), HCO+(J=1-0), and ^{12}CO(J=1-0) available in the literature for these galaxies, and compiled our sample in Table 1.

Most of the HCN data were taken from Liu et al. (2015). For the unreported values, we estimated the HCN and CO luminosities using the same equation as in Liu et al. (2015), as reported in our eq.(1). The references for all sources are provided in Table 1. Liu et al. (2015) used the following equation to calculate the line luminosity for CO and HCN:

$$L_{HCN,CO}(\mathbf{K}kms^{-1}pc^2)^{-1} = 3.25 \times 10^7 \times S_{HCN,CO}\Delta v \times v_{obs}^{-2} \times D_L^2, \tag{1}$$

where $S_{HCN,CO}\ \Delta v$ is the velocity integrated flux of HCN and/or CO lines in Jykms^{-1}, v_{obs} is the observed frequency for HCN (88.63 GHz), for CO (115.27 GHz), and D_L is the luminosity distance in Mpc. HCO+ luminosities were also calculated using eq.(1) with $v_{obs} = 89.19$ GHz. The uncommon unit of $L_{HCN,CO,HCO+}$ (Kelvin kilometer parsec squared per second) is due to spectral observation methods used in millimeter range, where the integration of brightness temperature with respect to the emission velocity is usually used to express line intensity Solomon et al. (1997). $\log_{10}(L_{HCN}/\mathbf{K}kms^{-1}pc^2)$ ranges from 5.6 to 9.1 with a mean of 7.5 , while $\log_{10}(L_{HCO+}/\mathbf{K}km\ s^{-1}pc^2)$ ranges from 5.9 to

9 with a mean of 7.4. Our maser sample contains 17 megamaser galaxies (MM, $\log_{10}(L_{H_2O}/L_\odot) \geq 1$) and 13 kilomaser galaxies (KM, $\log_{10}(L_{H_2O}/L_\odot) < 1$), the maximum value of $\log_{10}(L_{H_2O}/L_\odot)$ is 3.3 for the centre of the ultra luminous infrared galaxy (ULIRG) UGC5101, and the minimum is -2 in the nearby starburst galaxy IC342, the average of $\log_{10}(L_{H_2O}/L_\odot)$ is 1.

3   ANALYSIS OF THE DATASET

We use non-parametric statistics in order to analyse our relatively small sample. Most often, non-parametric statistics are based on ranks of the two variables (let's say x and y) rather than their values, where x_i and y_i are ordered increasingly and given ranks, then an analysis is carried out on these ranks rather than the data themselves. The power of using rank order analyses is shown when we have outliers (or anomalous points), avoiding the use of means of the variables x_i and y_i and their standard deviations (which is essentially the case in parametric analyses). This allows us to include outliers in the analysis without affecting the actual regression line of the relation (Kandalyan & Al−Zyout 2010a; Kandalyan & Al−Zyout 2010b). The Spearman's rank correlation coefficient, ρ, is the parametric Pearson correlation coefficient for the ranking of the x_i and y_i variables (see e.g. Conover 1981; Myers et al. 2013) and can be calculated as follows:

$$\rho = \frac{\sum_{i=1}^n (R_{x_i} - \overline{R_x})(R_{y_i} - \overline{R_y})}{\sqrt{\sum_{i=1}^n (R_{x_i} - \overline{R_x})^2 \cdot \sum_{i=1}^n (R_{y_i} - \overline{R_y})^2}}, \tag{2}$$

where the ranks R_{x_i} and R_{y_i} are the position of the ith x and i^{th} y variables in the sample, respectively, after ordering it, n is the sample size, $\overline{R_x}$ and $\overline{R_y}$ are the mean values of the ranks of the variables x and y, respectively. We calculated the Spearman rank-order correlation coefficients between the luminosity fractions given in Table 1 and present the non-parametric statistical results in Table 2.

Table 2 shows the Spearman's rank correlation coefficient ,ρ, between the variables and P-value of the corresponding ρ. Also shown in Table 2 is the result of Kendall-Theil Line regression (Kandalyan & Al−Zyout 2010a) including the slope of the linear regression line S, intercept I, 95% confidence interval for the slope, and the median deviation d.

It should be taken into consideration that luminosities of maser and dense gas tracers depend significantly on the distance to the sources. Thus, if both of the variables being analysed depend on the redshift z, the so-called Malmquist effect (Butkevich et al. 2005) should be eliminated first. For this purpose, we normalised the luminosities to L_{CO} to get the intrinsic relation between the variables without being affected by the distance. Using $L_{CO(1-0)}$ as a normaliser is very helpful because this molecule has a low dipole moment $\mu \approx 0.11$ D and low critical density, $n_{crit} \approx 2.2 \times 10^3$ cm^{-3} at T≈30K as it is estimated by Yang et al. (2010). These conditions are essentially satisfied in any molecular gas cloud, that is why CO(1-0) is used as a lower-density gas tracer. Normalising dense gas tracer luminosity to L_{CO} gives us the dense gas ratio in galaxies. The Central R Archive Network

---

[1] https://safe.nrao.edu/wiki/bin/view/Main/PublicWaterMaserList

R CRAN's package GGPUBR[2] was used to calculate Spearman correlations Alboukadel Kassambara (2020), and KTRLINE software[3] Granato, G.E. (2006) for Kendall-Theil analyses.

Table 1. The 30 H_2OMM data sample

Galaxy name	z	D_L	$\log_{10}(L_{H_2O}/L_\odot)$	$\log_{10}(L_{HCN}/\mathbf{K}kms^{-1}pc^2)$	$\log_{10}(L_{HCO+}/\mathbf{K}kms^{-1}pc^2)$	$\log_{10}(L_{CO}/\mathbf{K}kms^{-1}pc^2)$	$\log_{10}(L_{H_2O}/L_{CO})$	$\log_{10}(L_{HCN}/L_{CO})$	$\log_{10}(L_{HCO+}/L_{CO})$	References
NGC 23	0.015231	62.4	2.26	7.81	**	9.21	-6.95	-1.4	**	1,3,**,3
NGC 17 (NGC34)	0.019617	80.92	0.95	8.95	**	9.55	-8.6	-0.6	**	2,3,**,3
NGC 253	0.000811	4.11	-0.7	7.82	7.37	9.18	-9.88	-1.36	-1.82	1,3,4,3
NGC 520	0.007609	30.59	0	7.79	**	9.46	-9.46	-1.67	**	1,3,**,3
NGC 613	0.00494	20.9	1.3	7.43	**	8.54	-7.24	-1.11	**	1,5,**,11
NGC 1068	0.003793	15.46	2.2	8.48	8.15	9.47	-7.27	-0.99	-1.32	1,3,6,3
IC 342	0.000103	4.32	-2	7.6	6.54	9.21	-11.21	-1.61	-2.67	1,3,6,3
NGC 2146	0.002979	15.34	0	8.01	7.28	9.16	-9.16	-1.15	-1.88	1,3,6,3
NGC 2273	0.006138	28.54	1.51	7.32	6.84	7.88	-6.37	-0.56	-1.03	1,3,7,3
He 2-10	0.002912	12	-0.15	6.6	6.81	8.32	-8.47	-1.72	-1.51	1,3,8,3
UGC 5101	0.039367	164.93	3.28	9.07	8.48	9.69	-6.41	-0.62	-1.21	1,3,9,3
M 82 (NGC3034)	0.000677	4.89	0	7.65	7.26	9.01	-9.01	-1.38	-1.77	1,3,6,3
NGC 3079	0.003723	19.51	2.7	7.59	7.63	9.01	-6.31	-1.42	-1.38	1,12,12,11
NGC 3256	0.009354	35.86	1	8.39	8.5	9.67	-8.67	-1.28	-1.17	1,3,6,3
NGC 3556	0.002332	12.09	0	6.28	6.48	8.57	-8.57	-2.29	-2.09	1,12,12,3
NGC 3620	0.005604	19.18	0.6	7.82	6.88	8.71	-8.11	-0.89	-1.83	1,3,13,3
Arp 299	0.010411	48.02	2.1	8.42	8.26	9.54	-7.44	-1.12	-1.28	1,3,6,3
NGC 4038 (NGC4039)	0.005688	21.1	0.9	7.2	7.68	9.1	-8.2	-1.9	-1.41	1,3,6,3
NGC 4051	0.002336	9.9	0.3	5.57	5.92	7.63	-7.33	-2.06	-1.71	1,7,7,11
NGC 4258	0.001494	6.1	1.9	6.39	6.61	7.76	-5.86	-1.37	-1.15	1,14,14,15
NGC 4388	0.008419	34.8	1.08	6.93	7.29	8.68	-7.6	-1.75	-1.39	1,14,14,11
NGC 4945	0.001878	5.2	1.7	7.67	7.7	9.2	-7.5	-1.53	-1.5	1,3,6,3
NGC 5128(Centaurus-A)	0.001823	7.7	0	6.26	6.29	8.2	-8.2	-1.94	-1.91	2,16,16,11
M 51 (NGC5194)	0.001544	7.53	-0.22	6.78	**	9.15	-9.37	-2.37	**	1,3,**,3
NGC 5256	0.027863	121.77	1.51	8.11	8.42	9.88	-8.37	-1.77	-1.46	1,3,17,3
NGC 5347	0.007789	32.18	1.51	7.2	**	7.59	-6.08	-0.39	**	1,3,**,3
Circinus	0.001448	6.1	1.3	7.23	**	8.41	-7.11	-1.18	**	1,19,**,11
NGC 5506	0.006181	25.5	1.7	6.63	6.93	7.8	-6.1	-1.17	-0.9	1,14,14,20
NGC 6240	0.02448	106.71	1.6	8.89	8.99	9.92	-8.32	-1.03	-0.93	1,12,21,3
NGC 7479	0.007942	33.56	1.28	7.97	**	9.36	-8.08	-1.39	**	1,3,**,3

Note. Columns shown in the Table are: (1) Name of the galaxy. (2) Redshift, z taken from Preferred redshift from NASA/IPAC Extragalactic Database (NED)(https://ned.ipac.caltech.edu/). (3) Luminosity distance, D_L in Mpc, when available, taken from Liu et al. (2015), otherwise calculated using NED cosmology calculator (http://www.astro.ucla.edu/ wright/CosmoCalc.html) adopting flat cosmology. (4) Isotropic H_2O maser luminosity logarithm, $\log_{10}(L_{H_2O}/L_\odot)$. (5) HCN(J=1-0) line luminosity logarithm, $\log_{10}(L_{HCN}/\mathbf{K}kms^{-1}pc^2)$. (6) HCO+(J=1-0) line luminosity logarithm, $\log_{10}(L_{HCO+}/\mathbf{K}kms^{-1}pc^2)$. (7) ^{12}CO(J=1-0) line luminosity logarithm, $\log_{10}(L_{CO}/\mathbf{K}kms^{-1}pc^2)$. (8) Normalized H_2O maser emission luminosity (L_{H_2O}/L_{CO}) logarithm. (9) Normalized HCN line luminosity (L_{HCN}/L_{CO}) logarithm. (10) Normalized HCO+ line luminosity (L_{HCO+}/L_{CO}) logarithm. (11) References for the H_2O, HCN, HCO+ and CO luminosities, respectively, ** stands for not available observation or reference.

References. H_2O data: (1) "https://safe.nrao.edu/wiki/bin/view/Main/PublicWaterMaserList", (2) Kuo C. Y., et al. (2018). HCN, HCO+ and CO data: (3) Liu et al. (2015), (4) Knudsen et al. (2007), (5) Lindberg et al. (2011), (6) Baan et al. (2008), (7) Sani et al. (2012), (8) Imanishi et al. (2007), (9) Imanishi et al. (2006), (10) Koda et al. (2002), (11) Israel (2020), (12) Costagliola et al. (2011), (13) Green et al. (2016), (14) Jiang et al. (2011), (15) Krause et al. (2007), (16) McCoy et al. (2017), (17) Querejeta et al. (2016), (18) Imanishi et al. (2009), (19) Curran et al. (2001), (20) Raluy et al. (1998), (21) Greve et al. (2009).

Table 2. Correlation and regression results.

	For all data sample:	
	$\log_{10}(L_{HCN}/L_{CO})$	$\log_{10}(L_{HCO+}/L_{CO})$
$\log_{10}(L_{H_2O}/L_{CO})$	N = 30	N = 22
	$\rho = 0.38$	$\rho = 0.66$
	P = 1.9×10^{-2}	P = 4.5×10^{-4}
	S = 1.03	S = 2.36
	I = -6.67	I = -4.77
	$-6.67 \leq S \leq 1.71$	$1.41 \leq S \leq 3.42$
	d = 0.43	d = 0.53
	For sources with normal IR luminosity:	
	$\log_{10}(L_{HCN}/L_{CO})$	$\log_{10}(L_{HCO+}/L_{CO})$
$\log_{10}(L_{H_2O}/L_{CO})$	N = 21	N = 15
	$\rho = 0.56$	$\rho = 0.83$
	P= 4.4×10^{-3}	P= 5.8×10^{-5}
	S = 1.31	S = 2.71
	I = -5.74	I = -3.53
	$0.22 \leq S \leq 2.06$	$1.56 \leq S \leq 3.96$
	d = 0.08	d = -0.04

Note. N is the sample number. Spearman's rank correlation results: ρ is the rank correlation coefficient between the variables and P is the P-value of the corresponding ρ, we consider the value P$\leq$0.05 for significant correlations. Kendall-Theil linear regression results: S is the slope of the regression line, I is the intercept, 95% percent confidence interval of slope is given as a range of S, and the median deviation d.

4 DISCUSSION

We expect H_2O maser emission to be correlated with the dense gas fraction in AGNs, for reasons introduced in Section 1. The dense gas fraction is usually expressed by the ratio of the line luminosity of one of the dense gas tracer molecules such as HCN, HCO+, CS, HNC, N_2H+ to the line luminosity of one of the low-density gas tracers such as CO and C I (neutral atomic carbon) lines. On the grounds that the CO emission line is the most effectively observed, we used it to calculate the dense gas fraction for our sample.

As shown in Table 2, both HCN and HCO+ dense gas fractions correlate with (L_{H_2O}/L_{CO}) with Spearman's correlation coefficients equal to 0.38 and 0.66 respectively. However, HCO+ seems to be strongly correlated with L_{H_2O}/L_{CO} while L_{HCN} / L_{CO} shows a weaker correlation, with regression line equations

$$\log_{10}(L_{H_2O}/L_{CO}) = 1.03 \log_{10}(L_{HCN}/L_{CO}) - 6.67, \quad (3)$$

$$\log_{10}(L_{H_2O}/L_{CO}) = 2.36 \log_{10}(L_{HCO+}/L_{CO}) - 4.77. \quad (4)$$

Fig. 1 and Fig. 2 display eq.(3) and eq.(4), respectively.

We further investigated these correlations after eliminating the sources with only HCN measurements available. We find that there is no more correlation between L_{H_2O}/L_{CO} and L_{HCN}/L_{CO} ($\rho = 0.27$ and P = 0.23). This result casts doubts on HCN as an accurate and unbiased dense gas tracer in maser sources.

Following the results reported by other authors (e.g. Gracia et al. 2006, Papadopoulos 2007), the luminous and ultraluminous IR galaxies ((U)LIRG) show a noticeable enhancement of HCN that could not be necessarily related to
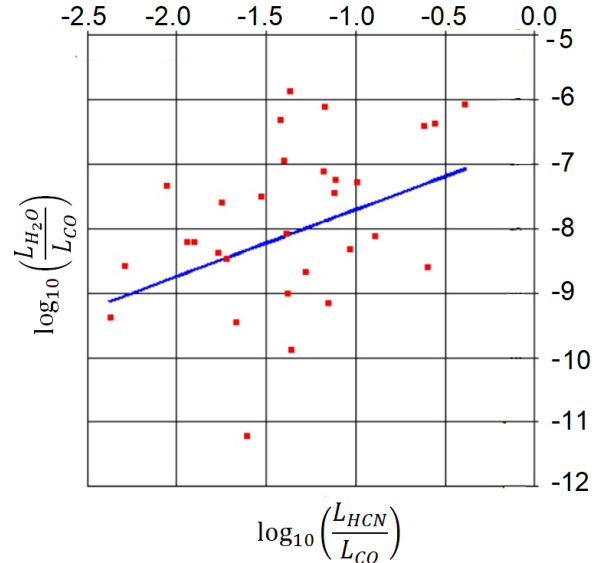
Figure 1. Relation between L_{H_2O}/L_{CO} and L_{HCN}/L_{CO} in logarithm scale. The blue line is the Kendall-Their regression line of the relation (see eq.(3)).
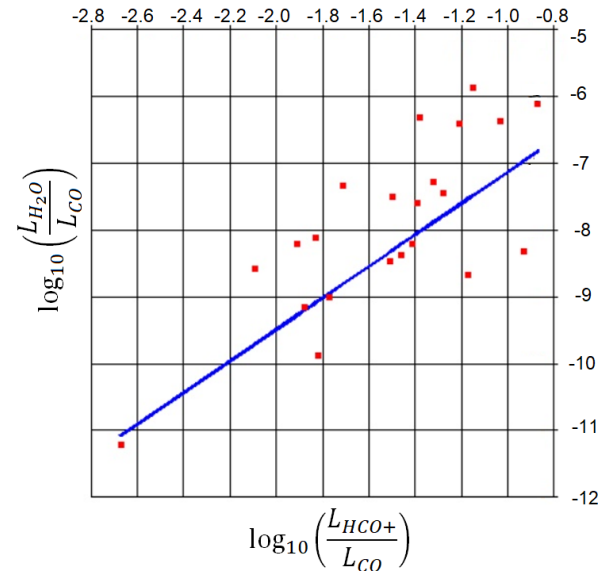

Figure 2. Relation between L_{H_2O}/L_{CO} and L_{HCO+}/L_{CO} in logarithm scale. The blue line is the Kendall-Theil regression line of the relation. A comparison with Fig.1 clearly shows how HCO+ interrelates with maser emission stronger than HCN (see eq.(4)).

dense gas, so it might not be a useful tool to use HCN as a dense gas tracer in these kind of galaxies. Rather, it is much safer to use HCO+ or high-level transitions of HCN and HCO+ such as HCN(J=2-1), HCN(J=3-2) and HCO+(J=3-2). We also tried to find the correlation after excluding (U)LIRG sources, which roughly represent only one third
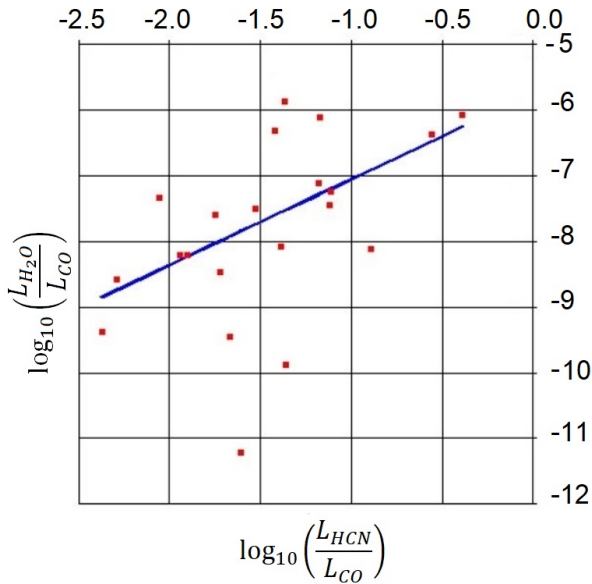
Figure 3. Relation between maser emission and the dense gas fraction as extracted from HCN for normal IR radiation galaxies. The blue line is the Kendall−Theil regression line of the relation. (See Table 2)

Figure 4. Relation between maser emission and the dense gas fraction as extracted from HCO+ for normal IR radiation galaxies. The blue line is the Kendall−Theil regression line of the relation. (See Table 2)

of the sample. L_{HCN}/L_{CO} was found to be moderately correlated with maser emission, with a sample number of 21 out of 30, and a $\rho = 0.56$, P= 4×10^{-3} as it is plotted in Fig. 3 and Fig. 4. Also it is worth noticing that HCO+ correlates better with maser emission after removing (U)LIRG (N= 15, ρ 0.83, and P= 6×10^{-5}). This agrees with the results of Papadopoulos (2007) and it may indicate the presence of turbulent molecular gas which can dilute the presence of HCO+ gas.

Another factor that may affect the abundance of HCN relative to HCO+ is metallicity of the emitting source, in fact the abundance of HCN as a nitrogen bearing molecule decreases faster than HCO+ in low-metallicity CND environments (Braine et al. 2017, Kepley et al. 2018). Unfortunately, we cannot currently rule out this effect due to the small sample size but it would be possible to check for the metallicity effect on HCN/HCO+ ratios both at nuclei and at CND for H_2OMM galaxies in further studies.

Fig. 5 and Fig. 6 show the box and whisker plot of maser types versus the dense gas luminosity fraction of HCN and HCO+, respectively. As it can be seen, the HCO+ dense gas fraction is slightly better distinguished between the two types of masers than the HCN dense gas fraction, with a tendency to be higher in MM sources in both cases.

In addition, a comparison of the ranges of the dense gas ratios in Fig. 5 and Fig. 6 immediately reveals the widest range is for HCN dense gas fraction in KM, this might be fairly interpreted as high enhancement of HCN in KMs. Gracia et al. (2006) discussed observational evidences of HCN enhancement in high-mass star-formation regions, and since KMs are generally powered by starbursts, thus the embedded massive star-formation regions in galaxies with KM emission might be the reason of the wide range of HCN dense gas ratio.

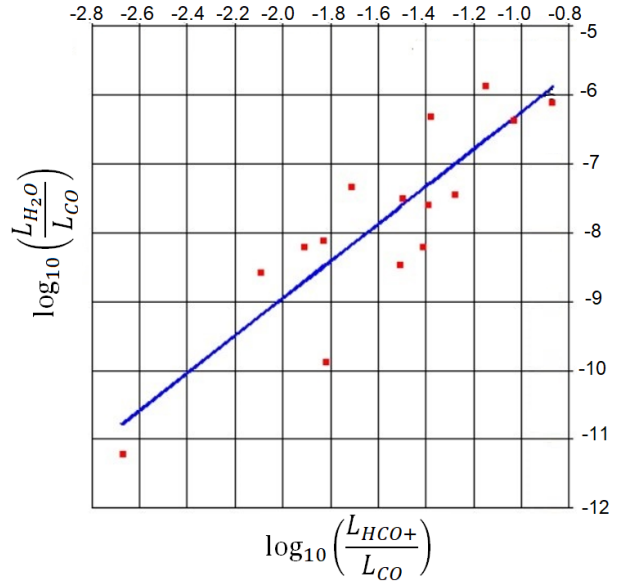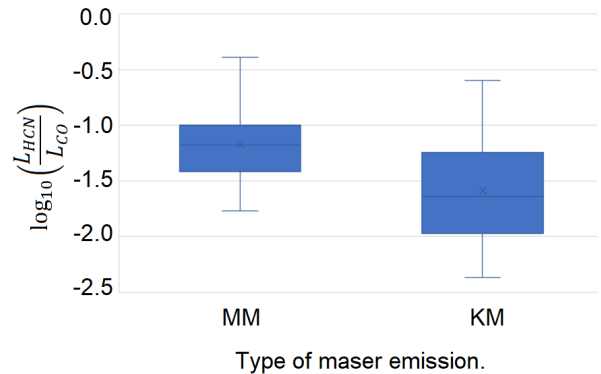Besides, the critical density of HCN was found to be two

Figure 5. The box and whisker plot of maser types versus the HCN dense gas fraction in both type of megamaser galaxies: kilomasers (KM) and megamasers (MM).

order of magnitude less than what is commonly accepted ($n_{crit} \sim 10^5$ cm^{-3}) (Kauffmann et al. 2017). If this is the case, then HCN should not be considered as a dense gas tracer in extragalactic sources.

Consequently, our results show that HCO+ rather than HCN is the molecular gas to be looked for if we want to place constraints on sources to survey for megamasers.

5 CONCLUSIONS

HCN and HCO+ dense gas fractions in 30 water vapor megamaser galaxies have been statistically analysed. Both fractions show a correlation with water maser emission, with HCO+ being stronger than HCN. Moreover, after remov-
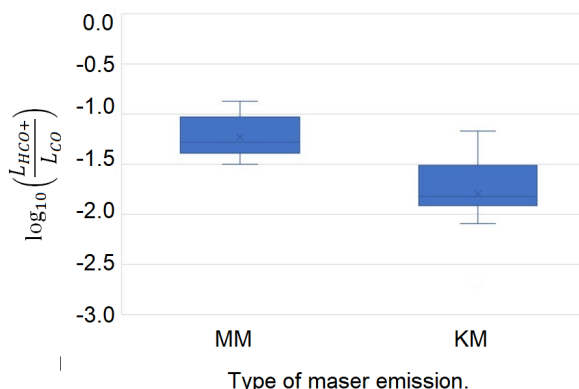
Figure 6. The box and whisker plot of maser types versus the HCO+ dense gas fraction in both type of megamaser galaxies: kilomasers (KM) and megamasers (MM). When compared with Fig. 5, the tow types of maser are more distinguished here.

ing (U)LIRG sources, the HCO+ correlation becomes very tight and HCN correlation becomes stronger. Our results agree with previous works on dense gas as a favorable parameter to be used in water megamaser surveys performed by Zhang et al. (2009) and Huang et al. (2014). According to our analyses, HCO+ is preferable on HCN as a dense gas tracer in megamaser sources. A further study for high level transitions would help to better elucidate the circumstances in which each of these dense gas tracers could be reliable as a tracer to dense gas in maser vigorous sources.

ACKNOWLEDGEMENTS

DATA AVAILABILITY

The data used in this study will be made available by the corresponding authors upon request.

REFERENCES

Baan W. A., Henkel C., Loenen E., 2008, EAS Publications Series, 31, 111
Braatz J. A., Wilson A. S., Henkel C., 1997, ApJS, 110, 321
Braine J., Shimajiri Y., André P., Bontemps S., Gao Y., Chen H., Kramer C., 2017, A&A, 597, A44
Butkevich A. G., Berdyugin A. V., Teerikorpi P., 2005, MNRAS, 362, 321
Castangia P., Panessa F., Henkel C., Kadler M., Tarchi A., 2013, MNRAS, 436, 3388
Churchwell E., Witzel A., Huchtmeier W., Pauliny−Toth I., Roland J., Sieber W., 1977, A&A, 54, 969
Claussen M. J., Lo K.−Y., 1986, ApJ, 308, 592
Conover W. J., 1981, Technometrics, 23, 415
Constantin A., 2012, J. Phys.: Conf. Ser. 372, 012047

Costagliola F., Aalto S., Rodriguez M. I., Muller S., Spoon H. W. W., Martín S., Peréz-Torres M. A., Alberdi A., Lindberg J. E., Batejat F., Jütte E., Van Der Werf P., Lahuis F., 2011, A&A, 528, A30
Curran S. J., Johansson L. E. B., Bergman P., HeikkilÃd' A., Aalto S., 2001, A&A, 367, 457
Gao Y., Solomon P. M., 2004, ApJS, 152, 63
GGPUBR: 'ggplot2' Based Publication Ready Plots. R package version 0.3.0. https://CRAN.R-project.org/package=ggpubr
GraciÃą-Carpio J., GarcÃ■a-Burillo S., Planesas P., Colina L., 2006, ApJ, 640, 135
Green C. -E., Cunningham M. R., Green J. A., Dawson J. R., Jones P. A., López−Sánchez Á. R., Verdes−Montenegro L., Henkel C., Baan W. A., Martín S., 2016 MNRAS, 457, 2470
Greenhill L. J., Tilak A., Madejski G., 2008, ApJ, 686, L13
Greve T. R., Papadopoulos P. P., Gao Y., Radford S. J. E., 2009, ApJ, 692, 1432
Huang F., Zhang J. S., Li R. M., Li H. K., 2014, J. Astrophys. Astron., 35, 509
Imanishi M., Nakanishi K., Kohno K., 2006, AJ, 131, 2888
Imanishi M., Nakanishi K., Tamura Y., Oi N., Kohno K., 2007, AJ, 134, 2366
Imanishi M., Nakanishi K., Tamura Y., Peng C. H., 2009, AJ, 137, 3581
Israel F. P. , 2020, A&A, 635, 131
Jiang X., Wang J., Gu Q., 2011, MNRAS, 418, 1753
Kandalyan R. A., Al−Zyout M. M., 2010, Astrophysics, 53, 329
Kandalyan R. A., Al−Zyout M. M., 2010,Astrophysics, 53, 475
Kauffmann J., Goldsmith P. F., Melnick G., Tolls V., Guzman A, Menten K. M., 2017, A&A, 605, L5
Kendall-Theil Robust Line (KTRLineâĂŤversion 1.0)âĂŤA visual basic program for calculating and graphing robust non-parametric estimates of linear-regression coefficients between two continuous variables: Techniques and Methods of the U.S. Geological Survey, book 4, chap. A7, 31 p.
Kepley A. A., Bittle L., Leroy A. K., Jiménez−Donaire M. J., Schruba A., Bigiel F., Gallagher M., Johnson K., Usero A., 2018, ApJ, 862, 120
Knudsen K. K., Walter F., Weiss A., Bolatto A., Riechers D. A., Menten K., 2007, ApJ, 666, 156
Koda J., Sofue Y., Kohno K., Nakanishi H., Onodera S., Okumura S. K.,Irwin J. A., 2002, ApJ, 573, 105
Kondratko P. T., Greenhill L. J., Moran J. M., 2006, ApJ, 652, 136
Krause M., Fendt C., Neininger N., , 2007, A&A, 467, 1037
Kuo C. Y., Constantin A., Braatz J. A., Chung H. H., Witherspoon C. A., Pesce D., Impellizzeri C. M. V., Gao F., Hao L., Woo J.-H, Zaw I., 2018, ApJ, 860, 169
Kuo C. Y., Hsiang J. Y., Chung H. H., Constantin A., Chang Y.−Y., da Cunha E., Pesce D., Chien W. T., Chen B. Y., Braatz J. A., Zaw I., Matsushita S., and Lin J. C., 2020, ApJ, 892, 18
Leiter K., Kadler M., Wilms J., Braatz J., Grossberger C., Krauß F., Kreikenbohm A., Langejahn M., Litzinger E., Markowitz A., Müller C., 2017 Proceedings of the International Astronomical Union No. 336, 141
Lindberg J. E., Aalto S., Costagliola F., Pérez−Beaupuits J. -P., Monje R.,Muller S., 2011, A&A, 527, A150
Liu L., Gao Y., Greve T. R., 2015, ApJ, 805, 31
Liu Z. W., Zhang J. S., Henkel C., Liu J., Müller P., Wang J. Z., Guo Q., Wang J., Li J., 2016, MNRAS, 466, 1608
Liu Z. W., Zhang J. S., Henkel C., Liu J., Müller P., Wang J. Z., Guo Q., Wang J., Li J., 2017, MNRAS, 466, 1608
Lo K. Y., 2005, Annual Review of Astronomy and Astrophysics, 43, 625
McCoy M, Ott J., Meier D. S., Muller S., Espada D., Martín S., Israel F. P., Henkel C., Impellizzeri V., Aalto S., Edwards P. G., Brunthaler A., Neumayer N., Peck A. B., van der Werf P.,

Feain I., 2017, ApJ, 851, 76

Myers J. L., Well A. D., Lorch Jr R. F., 2013, Research Design and Statistical Analysis,Third Edition.

Papadopoulos P.P., 2007 ApJ, 656, 792

Querejeta M., Schinnerer E., García–Burillo S., Bigiel F., Blanc G. A., Colombo D., Hughes A., Kreckel K., Leroy A. K., Meidt S. E., Meier D. S., Pety J., Sliwa K., 2016, A&A, 593, 118

Raluy F., Planesas P., Colina L., 1998, A&A, 335, 113

Ramolla1 M., Haas M., Bennert V. N., Chini R., 2011, A&A, 530, 147

Sani E., Davies R. I., Sternberg A., Graciá–Carpio J., Hicks E. K. S., Krips M., Tacconi L. J., Genzel R., Vollmer B., Schinnerer E., García-Burillo S., Usero A., Orban de Xivry G., 2012, MNRAS, 424, 1963

Solomon P. M., Downes D., Radford S. J. E., Barrett J. W., 1997, ApJ, 478, 144

Spergel D. N., Bean R., Doré O., Nolta M. R., Bennett C. L. Dunkley J., Hinshaw G., Jarosik N. Komatsu E., Page L., Peiris H. V., Verde L., Halpern M., Hill R. S., Kogut A., Limon M., Meyer S. S., Odegard N., Tucker G. S., Weiland J. L. Wollack E., Wright E. L., 2007, ApJS, 170, 377

Van den Bosch R. C. E., Greene J. E., Braatz J. A., Constantin A., Kuo C.-Y., 2016, ApJ, 819, 11

Yang B., Stancil P. C., Balakrishnan N., Forrey R. C., 2010, ApJ, 718,1062

Zhang, J. S., Henkel C., Kadler M., Greenhill L. J., Nagar N., Wilson A. S., Braatz J. A., 2006, A&A, 450, 933

Zhang J. S., Henkel C., Guo Q., Wang J., 2012, A&A, 538, 152

Zhang J. S., Henkel C., Guo Q., Wang H. G., Fan J. H., 2009, ApJ, 708, 1528

Zhu G., Zaw I., Blanton M. R., Greenhil L. J., 2009, ApJ, 742, 73

This paper has been typeset from a TeX/LaTeX file prepared by the author.